Uhn Joo Na
Research Engineer

Alan B. Palazzolo
Professor

Texas A&M University,
Mech. Engineering,
College Station, TX 77843

Andrew Provenza
NASA Glenn Research Center,
Cleveland, OH

Test and Theory Correlation Study for a Flexible Rotor on Fault-Tolerant Magnetic Bearings

This paper provides a new algorithm and test verification for implementing fault-tolerant operation of magnetically suspended, flexible shaft, rotating machinery. The currents to the magnetic bearing are redistributed in a manner so that the bearing actuator preserves the same linearized magnetic forces after some of its coils experience failure. The algorithm that searches a database for the appropriate failure compensation matrix utilizes a Boolean description of the failure state to quickly locate and download its target. The test results are shown to have good agreement with the system simulation results presented.
[DOI: 10.1115/1.1467652]

1 Introduction

A magnetic bearing system acts actively to suspend a spinning rotor magnetically without physical contact, as well as to suppress vibrations. Magnetic bearings are filling a greater number of applications in industry since they have many advantages over conventional fluid film or rolling element bearings, such as lower friction losses, lubrication free, temperature extreme, quiet, high speed operation, and dynamic force isolation. Magnetic suspensions produce active damping and stiffness which arises from the control action, so system parameters can be designed to avoid resonance or to supply optimum damping through the resonances while in operation.

A conventional 8-pole heteropolar magnetic bearing with opposing C-cores requires 4 coil pairs or even 2 coil pairs, each driven by its power amplifiers. Thus failure of one of the coils or power amplifiers may result in a failure of the entire system. Highly critical applications of these machinery elements may demand a fault-tolerant control strategy. Fault-tolerant control of magnetic bearing systems provides continued operation of the bearing even if its power amplifiers or coils suddenly fail. A fault-tolerant magnetic bearing actuator is controlled with a combination of 8 independent currents (8 independent force sources) one for each pole. If some coils fail, the remaining coils must provide the magnetomotive forces to generate the desired magnetic forces.

There have been some previous efforts on the fault-tolerant control of magnetic bearing actuators. Lyons et al. [1] used a three control axis radial bearing structure with control algorithms for redundant force control and rotor position measurement. In this approach, if one of the coils fails, its entire control axis is shut down, while still maintaining control. Maslen and Meeker [2], and Meeker [3] showed that a magnetic bearing with multiple coil failure can produce decoupled control forces if the remaining coil currents are properly redistributed. The flux coupling between poles in a heteropolar magnetic bearing and reassigning of the remaining coil currents provides a mean to produce desired force resultants in the x and y directions when some coils fail. The fault tolerant magnetic bearing system was demonstrated on a large flexible-rotor test rig in [4]. Na and Palazzolo [5,6] showed that the fault-tolerant control could be maintained for an 8-pole magnetic bearing including material path reluctances for up to 5 coils out of 8 failed. However, flux coupling with independent currents results in electromagnetic instability, which requires decoupling chokes [3]. All coils from the magnetic bearing are wound around a common, external electromagnetic core (a decoupling choke), then return to their power amplifiers. Na and Palazzolo [7] suggested the fault-tolerant magnetic bearings with reduced controller outputs and no decoupling chokes.

The fault tolerance described in this paper is achieved at the expense of additional hardware requirements such as 8 independent power amplifiers and a decoupling choke per magnetic bearing, fault detection system, and additional DSP controller channels. Only control dependent magnetic forces are decoupled with the bias linearization method suggested by previous works [2–6]. Since no condition is imposed on the position dependent forces, the position dependent magnetic forces may still be coupled. The present work provides a novel algorithm for the determination of the optimized redistribution of currents after the magnetic bearing actuator failure, such that the same magnetic forces are preserved. However, the overall load capacity of the bearing is reduced as coils fail. The same magnetic forces are then preserved only up to the load capacity of the failed bearing actuator. Test results are included to demonstrate how the fault-tolerant algorithm was experimentally verified on a high speed, flexible rotor-magnetic bearing test rig at NASA Glenn.

2 Fault-Tolerant Magnetic Bearing Forces

The magnetic bearing shown in Fig. 1 consists of a magnetically permeable stator with multiple pole legs (a coil is wound on each pole) and a permeable rotor separated with an air gap between the pole legs and the rotor. Magnetic forces are determined from magnetic flux density which may be reduced by flux leakage, fringing, saturation of magnetic material, and eddy current effects. The flux density vector in the air gaps of an 8-pole heteropolar magnetic bearing is described as [6];

$$\mathbf{B}=V(x,y)I, \tag{1}$$

where the current vector is;

$$\mathbf{I}=[i_1,i_2,\ldots,i_8]^T \tag{2}$$

The currents are distributed to each pole such that bias currents are held constant, and control currents are varied with feedback control actions. The current vector is expressed as;

$$\mathbf{I}=Tv, \tag{3}$$

where the distribution matrix is;

$$T=\lfloor T_b \;\; T_x \;\; T_y \rfloor, \tag{4}$$

and the voltage vector is;

$$\mathbf{v}=[v_b,v_{cx},v_{cy}]^T \tag{5}$$

Contributed by the Technical Committee on Vibration and Sound for publication in the JOURNAL OF VIBRATION AND ACOUSTICS. Manuscript received May 2001; revised January 2002. Associate Editor: G. Flowers.

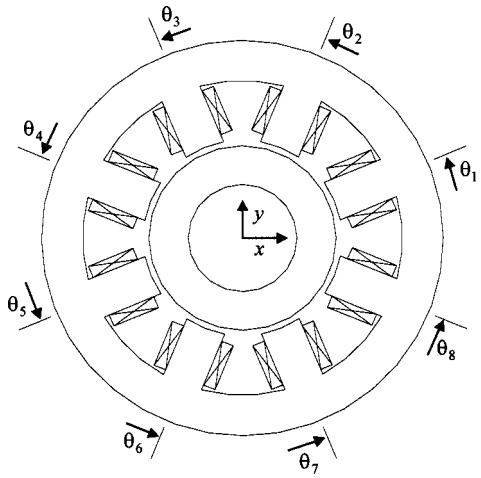

Fig. 1 Schematic of a heteropolar magnetic bearing

Two typical distribution schemes (coil winding schemes) are used for conventional bearings. The distribution schemes are;

$$T_1=\begin{bmatrix} 1 & 1 & 0 \\ -1 & 0 & -1 \\ 1 & 0 & 1 \\ -1 & 1 & 0 \\ 1 & -1 & 0 \\ -1 & 0 & 1 \\ 1 & 0 & -1 \\ -1 & -1 & 0 \end{bmatrix} \begin{matrix} N_x \\ S_y \\ N_y \\ S_x \\ N_x, \\ S_y \\ N_y \\ S_x \end{matrix} \quad T_2=\begin{bmatrix} 1 & 1 & 0 \\ 1 & 0 & 1 \\ -1 & 0 & -1 \\ -1 & 1 & 0 \\ 1 & -1 & 0 \\ 1 & 0 & -1 \\ -1 & 0 & 1 \\ -1 & -1 & 0 \end{bmatrix} \begin{matrix} N_x \\ N_y \\ S_y \\ S_x \\ N_x \\ N_y \\ S_y \\ S_x \end{matrix} \tag{6}$$

The feedback control voltages, determined from measured rotor motion, are distributed to each pole via T, and create an effective stiffness and damping of the bearing to suspend the rotor around the bearing center position. The magnetic forces including the distribution matrix are described as;

$$f_\eta = v^T U_\eta v \tag{7}$$

where

$$U_\eta = -T^T V^T \frac{\partial D}{\partial \eta} VT \tag{8}$$

$$D=\mathrm{diag}(g_j a/(2\mu_0)) \tag{9}$$

and where the air gap in the j-th pole is;

$$g_j = g_0 - x\cos\theta_j - y\sin\theta_j \tag{10}$$

The parameter η represents either x or y, and the parameters a, g_0, and μ_0 represent pole face area, nominal air gap, and permeability of air respectively. Magnetic forces are decoupled and linear with respect to the control voltages if any of the two distribution schemes, T_1 and T_2, is used for the bias linearization [8,9].

The distribution of currents can be designed as a part of a control law so that the effects of a coil failure can be very much mitigated with control action. Reassigning the remaining coil currents with a redefined distribution gain matrix in case of coil failures may provide the magnetic forces that compensate for the loss of coil currents [2–6]. If the distribution matrix T is determined such that U_η should be invariant through coil failures, the magnetic forces are then only dependent on the control voltage vector **v**. The nonlinear magnetic forces in Eq. (7) are linearized about the bearing center and zero control voltages.

$$\begin{bmatrix} f_x \\ f_y \end{bmatrix} = -\begin{bmatrix} k_{pxx} & k_{pxy} \\ k_{pyx} & k_{pyy} \end{bmatrix}\begin{bmatrix} x \\ y \end{bmatrix} + \begin{bmatrix} k_{vxx} & k_{vxy} \\ k_{vyx} & k_{vyy} \end{bmatrix}\begin{bmatrix} v_{cx} \\ v_{cy} \end{bmatrix}, \tag{11}$$

where

$$k_{p\eta\omega} = -\frac{\partial f_\eta}{\partial \omega} = -2T_b^T V \frac{\partial D}{\partial \eta}\frac{\partial V^T}{\partial \omega}\bigg|_{\substack{\eta=0 \\ \omega=0}} T_b v_b^2, \tag{12}$$

$$k_{v\eta\omega} = \frac{\partial f_\eta}{\partial v_{c\omega}} = -2T_b^T V^T \frac{\partial D}{\partial \eta} V\bigg|_{\substack{\eta=0 \\ \omega=0}} T_\omega v_b, \tag{13}$$

where the parameters η and ω both represent x or y direction. The distribution matrix T that produces the same linearized forces as those of an unfailed bearing is optimized with respect to preventing saturation using Lagrange Multiplier method [5,6].

Some examples of distribution matrices were calculated for the 8-pole heteropolar magnetic bearing used in the test, with $g_0(0.508\ \mathrm{mm})$, $a(602\ \mathrm{mm}^2)$, $n(50\ \mathrm{turns})$. The calculated distribution matrix for the 7-8th coils failed bearing is:

$$T_{78}=\begin{bmatrix} 2 & 1.5607 & -0.64578 \\ 2 & 1.0607 & 1.559 \\ 0 & 1.2071 & -0.50095 \\ 0 & 1.2071 & -0.50095 \\ 2 & -0.35355 & 0.14483 \\ 2 & 0.14645 & -2.06 \\ 0 & 0 & 0 \\ 0 & 0 & 0 \end{bmatrix} \tag{14}$$

and the 6-7-8th coils failed bearing is;

$$T_{678}=\begin{bmatrix} 2.3295 & 2.1526 & -0.85091 \\ 0.99961 & 1.3566 & -3.2971 \\ 3.0955 & 0.94629 & -2.2843 \\ 0.99961 & 1.3722 & -3.2906 \\ 2.3295 & -0.92037 & -2.1238 \\ 0 & 0 & 0 \\ 0 & 0 & 0 \\ 0 & 0 & 0 \end{bmatrix} \tag{15}$$

and the 2-4-6-8th coils failed bearing is;

$$T_{2468}=\begin{bmatrix} 1.8974 & 1.5916 & -0.02537 \\ 0 & 0 & 0 \\ -0.82814 & 0.72618 & -1.7532 \\ 0 & 0 & 0 \\ 1.8974 & -1.1075 & -1.1434 \\ 0 & 0 & 0 \\ 2.093 & 0.72618 & -1.7532 \\ 0 & 0 & 0 \end{bmatrix} \tag{16}$$

The linearized forces in Eq. (11) with any of the unfailed or failed distribution matrices, T_1, T_2, T_{78}, T_{678}, T_{2468}, and v_b of 4.851 result in $k_{pxx}=k_{pyy}$ of -1357931.2 N/m, $k_{vxx}=k_{vyy}$ of 131.38 N/Volt, $k_{pxy}=k_{pyx}$ of 0 N/m, and $k_{vxy}=k_{vyx}$ of 0 N/Volt. This shows that the linearized magnetic forces remains unchanged through a failure event if the distribution matrix for a specific failure is utilized.

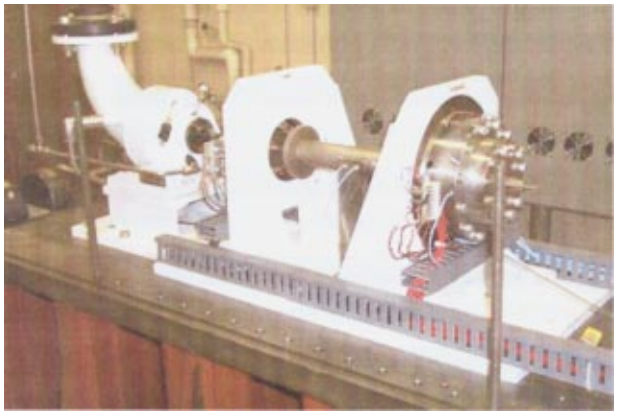

Fig. 2 Fault-tolerant magnetic bearing test rig

3 Flexible Rotor-Magnetic Bearing System Model

A horizontal flexible rotor test rig (Fig. 2) was built by NASA Glenn specifically for fault-tolerant magnetic bearing development. The flexible rotor has mass of 10.7 kg, length of 0.69 m. Two radial magnetic bearings are located at 0.1235 m from the ends. No thrust magnetic bearing is installed. The axial displacement is however limited by a simple mechanical stop and the reluctance centering effect of the two radial bearings. Two ball bearing type back-up bearings with the clearance of 0.000304 m (12 mils) are located outboard of the magnetic bearings. A finite element model of the flexible rotor with 38 elements is shown in Fig. 3. The flexible rotor is discretized into a reasonable number of elements which consist of a series of massless beam elements and lumped mass and inertias. The mass, polar moment of inertia, and transverse moment of inertia are halved and placed at each node. The equation of motion for the flexible rotor is then described as;

$$M\ddot{X}+G\dot{X}+KX=\mathbf{F}, \tag{17}$$

where M, G, and K represent mass, gyroscopic moment, and stiffness matrices respectively. External forces exerted on the system of equations are described as;

$$F=\mathbf{F}_m+\mathbf{F}_g+\mathbf{F}_u \tag{18}$$

$\mathbf{F}_m$, $\mathbf{F}_g$, and $\mathbf{F}_u$ represent magnetic force, gravity force, and unbalance force vectors respectively. The magnetic force vector is:

$$\mathbf{F}_m=H\tilde{F} \tag{19}$$

where

$$\tilde{\mathbf{F}}=[f_x^A \;\; f_y^A \;\; f_x^B \;\; f_y^B]^T$$

and where H is the 156×4 matrix that assigns magnetic forces to the corresponding states. Modal condensation technique is used to reduce the number of states in Eq. (17). The first r modes of the system below 2000 Hz are selected and normalized. $r\times1$ modal state vector $\mathbf{v}$ is defined as:

$$X(t)=\Psi\mathbf{v}(t) \tag{20}$$

Modal equations of motion for the flexible rotor is then described as:

$$\tilde{M}\ddot{\nu}(t)+\tilde{G}\dot{\nu}(t)+\tilde{K}\nu(t)=\tilde{F}(t), \tag{21}$$

where

$$\tilde{M}=\Psi^T M\Psi \tag{22}$$

$$\tilde{K}=\Psi^T K\Psi \tag{23}$$

$$\tilde{G}=\Psi^T G\Psi \tag{24}$$

$$\tilde{F}(t)=\Psi^T F(t) \tag{25}$$

4 Control System Design

The fault-tolerant control scheme consists of two independent parts, which are the fault-tolerant current distribution mechanism and a feedback voltage control law. The schematic of a fault-tolerant control scheme is shown in Fig. 4. The fault-tolerant current distribution system consists of fault detection, searching a database for the appropriate T, and implementation of T in the physical controller. Fault-initiating and detection mechanism are installed in the test rig. Coil failures are implemented by intentionally open-circuiting with computer controlled mechanical switches installed in all current paths. If a coil is open-circuited by turning off the corresponding switch, a TTL signal of 5 volt DC is

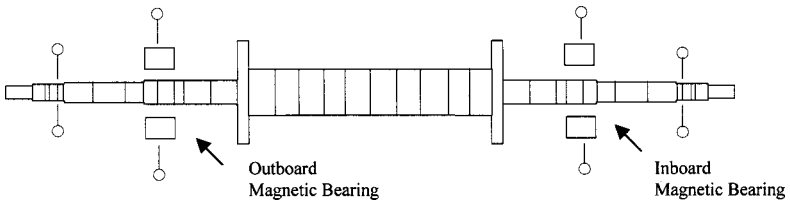

Fig. 3 Finite element model of the flexible rotor

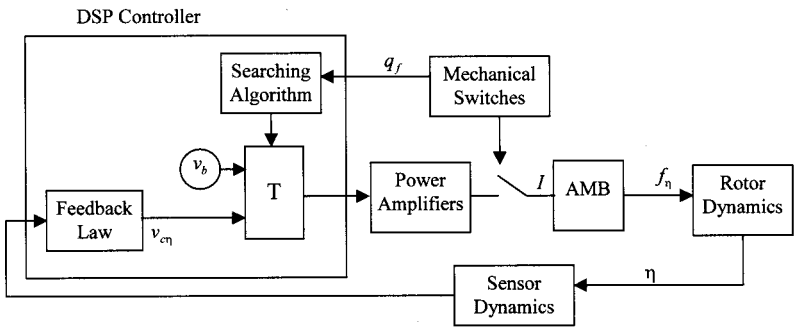

Fig. 4 Schematic of the fault-tolerant controller

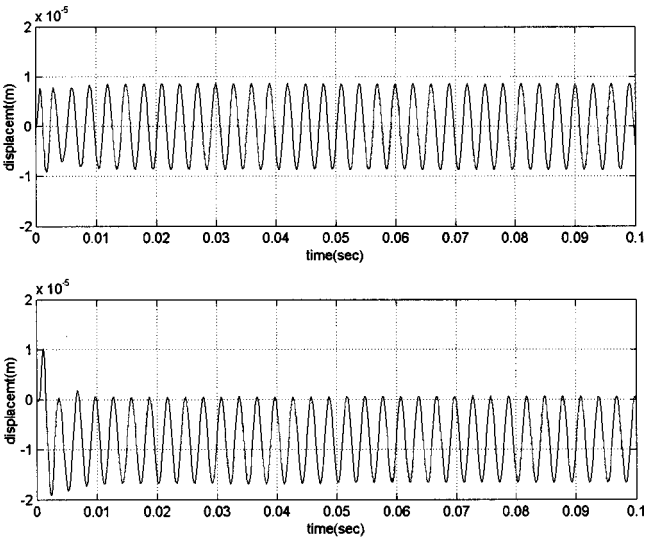

Fig. 5 Transient response of the rotor displacements at the outboard bearing

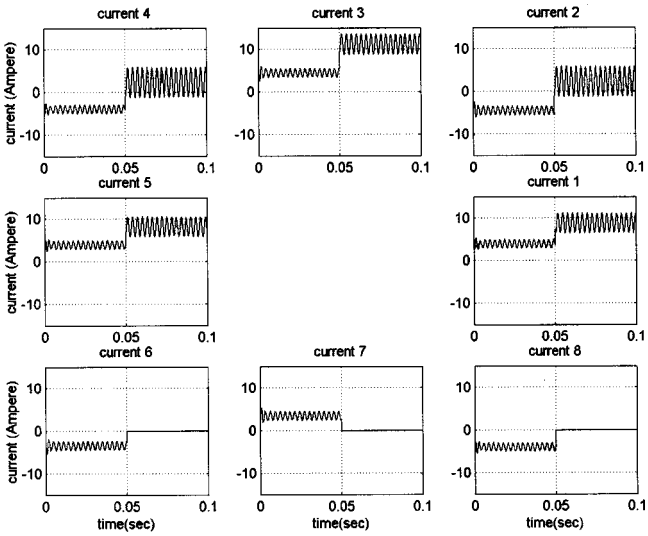

Fig. 7 Transient response of the current inputs to the outboard bearing

simultaneously supplied to the controller for fault detection. If a coil remains unfailed, a TTL signal of 0 volts is supplied to the controller. Failure status of all 8 coil currents can be continuously monitored in the DSP controller by TTL signals. A failure status vector can be generated in the DSP controller based on the measured TTL signals. An example of a measured failure status vector for the 6-7-8th coils failed is:

$$\mathbf{q}_f=[1\ \ 1\ \ 1\ \ 1\ \ 1\ \ 0\ \ 0\ \ 0]^T \tag{26}$$

Failure status vectors up to all combinations of 4 coils failed and certain combinations of 5 coils failed out of 8 coils are tabulated in a reference table such as;

$$Q=[q_1\ \ q_2\ \ \ldots\ \ q_{n-1}\ \ q_n] \tag{27}$$

The fault status table Q is stored in the DSP controller as a part of the searching algorithm. Distribution matrices T_i corresponding to q_i in Eq. (27) can also be calculated and tabulated as;

$$\underline{T}=[T_1\ \ T_2\ \ \ldots T_{n-1}\ \ T_n] \tag{28}$$

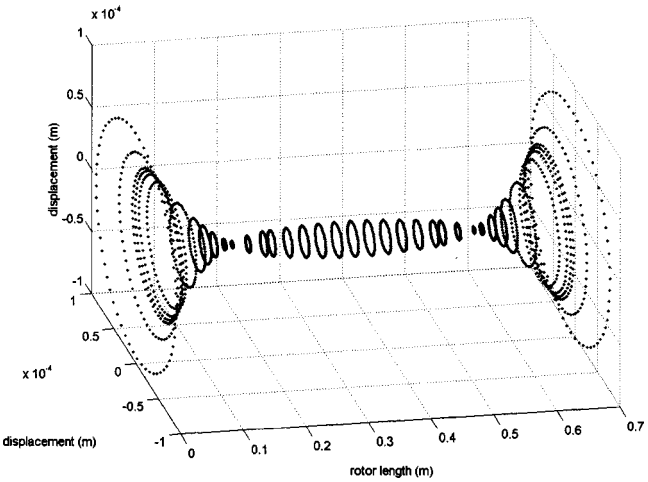

Fig. 6 Rotor whirling response at 20000 RPM

The measured failure status vector $\mathbf{q}_f$ is compared with q_i one by one. If q_f is matched to q_i, the i-th distribution matrix of T_i is implemented in the controller. A series of actions for failure detection, searching for T, and replacement by the new T occur in one loop time (70 microseconds, 14300 samples/sec) of the DSP controller.

The feedback voltage control law can be designed excluding all fault tolerance considerations since the actuator's force-voltage and force-displacement characteristics is unaltered by the failure. A feedback control law designed for an unfailed bearing actuator can be used during the failure events. For the tests in this paper a simple PD feedback control law was used.

$$v_{c\eta}=K_\rho\eta+K_d\dot{\eta} \tag{29}$$

The closed loop bearing stiffness and damping may be adjusted by tuning the PD control gains [10]. The feedback control law remains unaltered during the failure while the appropriate current distribution matrix T is continuously updated using the searching algorithm. The fault-tolerant current control law is then described as;

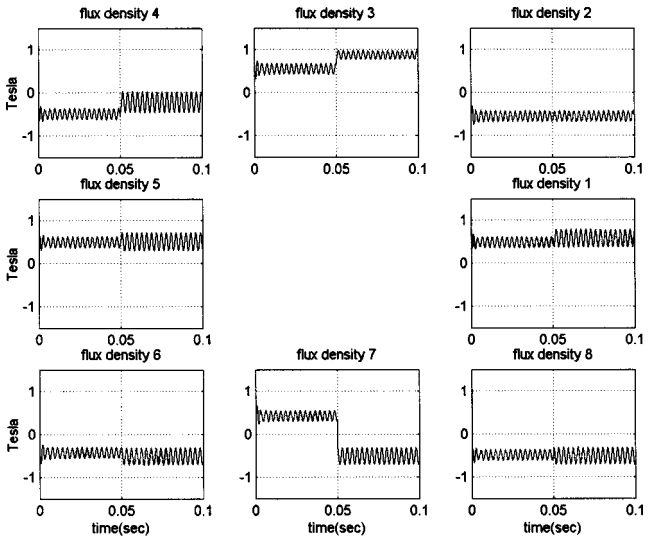

Fig. 8 Transient response of the flux densities at the outboard bearing

$$I = T_b v_b + [T_x T_y] \begin{bmatrix} v_{cx} \\ v_{cy} \end{bmatrix} \tag{30}$$

The adaptive distribution gain matrix keeps the nonlinear magnetic forces unaltered from coil failures while the voltage control law stabilizes the system.

5 Simulations

The coil failure event was simulated with a flexible rotor model and the fault-tolerant controller. The following system dynamics simulation illustrates the transient response of a rotor supported by magnetic bearings during a coil failure event. An unbalance force of $me\Omega^2$ with m (2.14 grams), e (0.01 m) and Ω (spinning speed) are applied at the two bearing locations. It is notable that although the algorithm presented preserves the linearized forces in Eq. (11) after coil failure, the simulation model employs nonlinear bearing forces as a more stringent test. The distribution matrix of T_1 was switched to T_{678} when 3 adjacent coils failed at 0.05 seconds while the same control gains were maintained during the failures. The undamped first bending critical speed of the rotor-bearing system model is 343 Hz (20600 RPM). The rotor speed was held constant at 20,000 RPM. Nonlinear magnetic forces are directly used so that flux density variation could be plotted and more accurate forces could be used. However, the system is designed using linear magnetic forces. Figure 5 shows transient response plots from the normal unfailed operation through the 6-7-8th coils of the outboard bearing failed at 0.05 sec. Rotor whirling response at 20,000 RPM is shown in Fig. 6. Transient response of the current inputs to the outboard bearing is shown in Fig. 7 and transient response of the flux densities in the outboard bearing is shown in Fig. 8.

6 Experiments

The fault-tolerant controller was tested on the test rig at NASA Glenn. A total of 10 channels of controller inputs to the dSPACE controller are required for each bearing (8 channels of TTL coil failure status signals and 2 displacement signals for a radial bearing). The 8 control outputs from dSPACE go to 8 independent power amplifiers which supply currents to each bearing. The failure tests were performed and recorded only on the outboard bearing.

Three adjacent coil currents of the 6-7-8th coils were turned off with mechanical switches at 2.395 seconds after starting data recorder while the rotor was spinning at 20,000 RPM. The TTL signals for failure status of the 8 coil currents were continuously monitored and supplied to the DSP controller. The displacement plots at the outboard bearing during the coil failure event are shown in Fig. 9. These plots showed subsynchronous vibrations as well as 1× vibrations. Very little transient response occurred for displacements during failure, but the y displacement did change slightly after 3 adjacent coils failed. The currents to the outboard bearing are shown in Fig. 10. A peak appeared during the transition after failure because the 3 mechanical switches were not turned off simultaneously. The TTL signals of the failure status shown in Fig. 9 indicated that there was 0.003 seconds interval between the first coil failure and the last two coil failures. Conse-

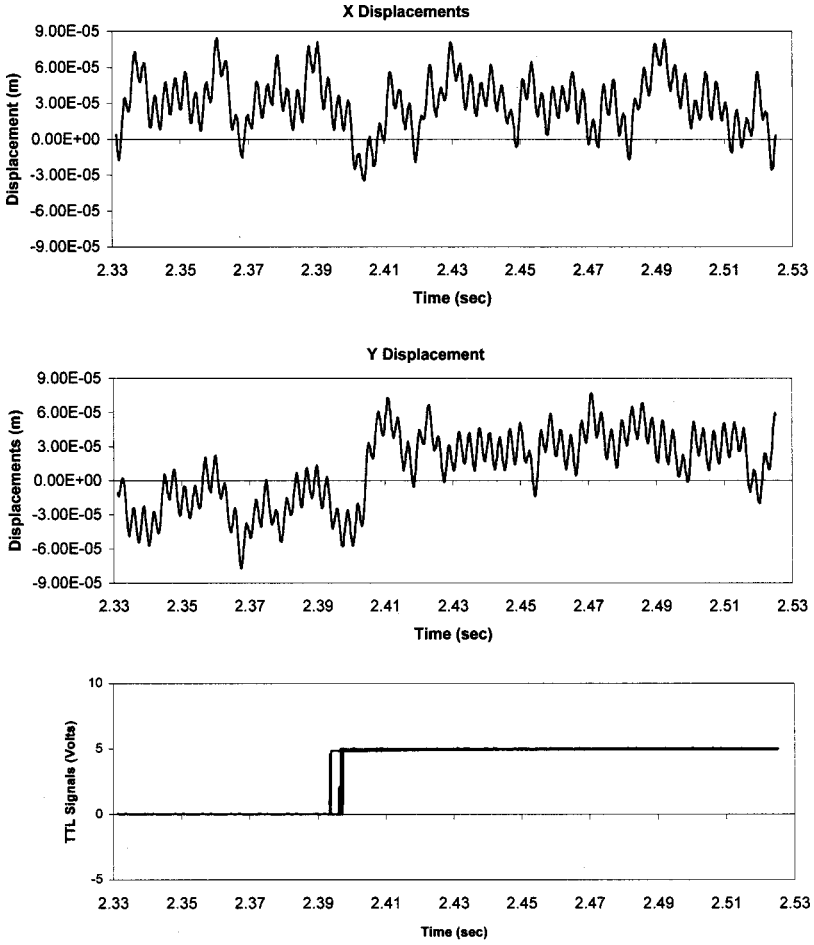

Fig. 9 Displacement plots (peak-peak) of 3 coils (the 6-7-8th coils) failed operation

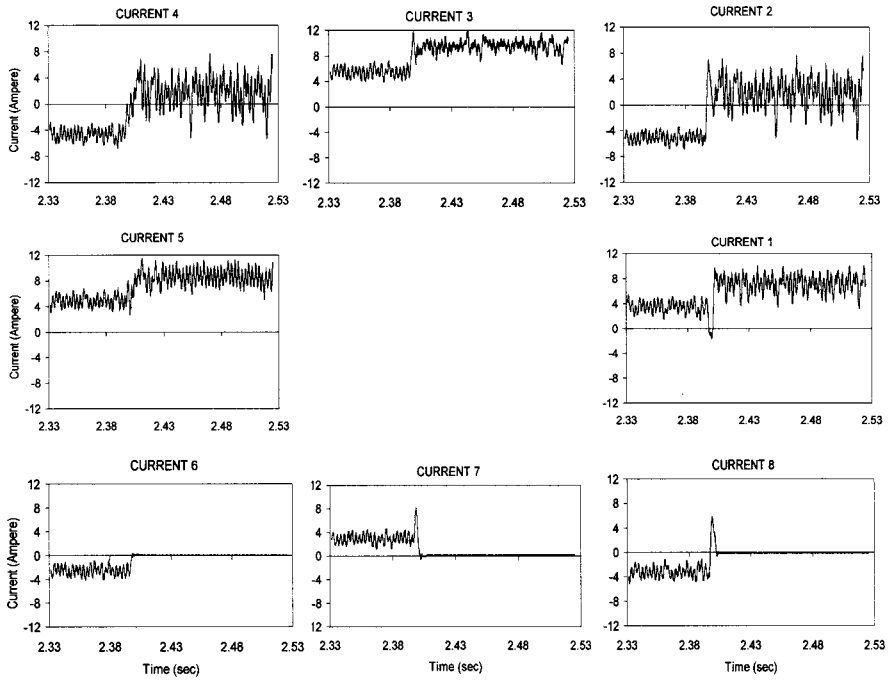

Fig. 10 Currents to the outboard bearing for 3 coils (the 6-7-8th coils) failed operation

quently, the search engine in the controller downloaded a distribution matrix for a single failure case first, and then T_{678} was downloaded shortly after two more failures were detected. The time delay due to fault detection and searching for T was negligible. The test results show good agreement with the simulation of the 6-7-8th coils failed operation in the previous section, i.e., compare Figs. 7 and 10.

A series of coil failures with up to 5 coils failed out of 8 coils was tested on the outboard bearing by turning off mechanical switches one by one. The same control gains were maintained throughout all of these coil failure events. Figure 11 shows snap shot plots of displacements, currents, and TTL signals at the outboard bearing at 18000 RPM throughout a series of coil failure events. The TTL failure status signals of failure showed that the 2nd coil failed at 0.605 seconds, then the 1st coil failed at 1.93 seconds, the 7th coil failed at 3.16 seconds, the 5th coil failed at 4.215 seconds, and the 4th coil failed at 5.31 seconds, respectively. It is interesting to see that no significant changes in displacements occurred during the failure events while the currents changed significantly. Although there did occur a short transient increase in vibration as shown in the (1, 4) plot of Fig. 11 it is gone in the (1, 5) plot. This means that the same closed loop dynamic response was successfully maintained during the failures without changing the feedback control gains. The currents were automatically adjusted with appropriate distribution matrices during the coil failure events.

7 Conclusions

A current distribution gain matrix, T is determined so that the bearing actuator will preserve the same total linearized magnetic forces even after some components such as coils or power amplifiers experience failure. Experiments show that rotor displacements after failure can be maintained close to the displacements before failure for up to all combinations of 4 coils failed and certain combinations of 5 coils failed out of 8 coils. The overall load capacity of the bearing is reduced as coils fail. The same magnetic forces are then preserved only up to the load capacity of the failed bearing actuator. Relatively large increase in currents and flux densities may be required to maintain the same closed loop dynamic properties after failure, depending on the nature of the disturbances. This would increase RMS power requirements to run in the failed condition. Therefore, disturbance levels from imbalance, runout or sideloads should still be maintained at low levels to prevent saturation.

Acknowledgments

The authors wish to extend their gratitude to NASA Glenn (NRA 99-GRC-2) U.S. Army at NASA Glenn (Gerald Montague and Albert Kascak) and the NAVY ONR (BAA 97-030) for support of this research.

Nomenclature

a = pole face area
$\mathbf{B}$ = flux density vector
D = air gap energy matrix
$\mathbf{F}$ = global force vector
f_η = magnetic force in the η direction
G = global gyroscopic matrix
g_0 = nominal air gap distance
$\mathbf{I}$ = current vector
i_j = current to the j-th pole
K = global stiffness matrix
K_p, K_d = feedback gains
$k_{p\eta\omega}$ = position stiffness
$k_{v\eta\omega}$ = voltage stiffness
M = global mass matrix
n = number of coil turns
$\mathbf{v}$ = voltage vector
v_b, v_{cx}, v_{cy} = bias, x control, and y control voltages
T = current distribution matrix
U_η = voltage to force matrix
V = current to flux density matrix
$\mathbf{X}$ = global displacement vector
x, y = rotor displacements
μ_0 = permeability of air
θ = pole face angle

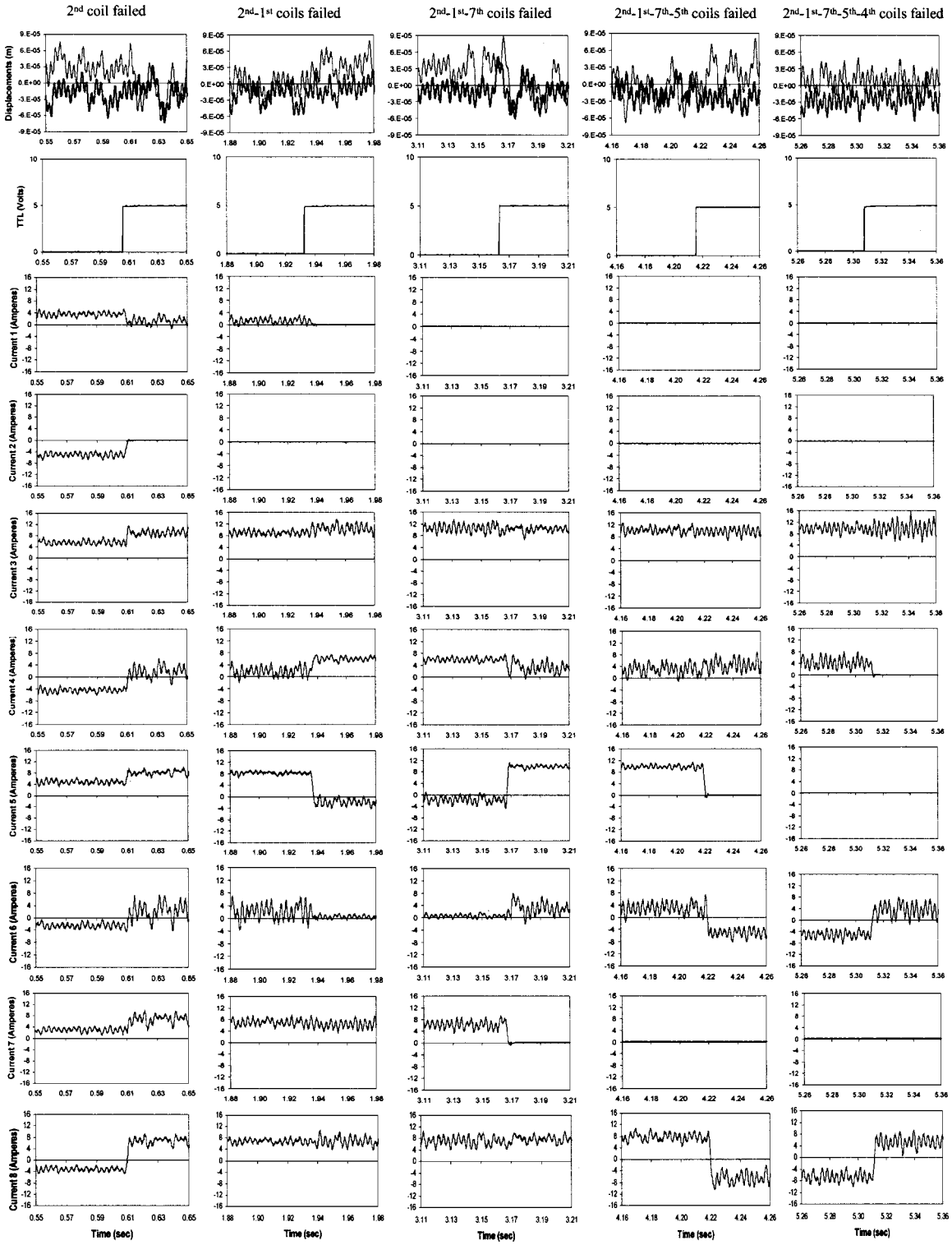

Fig. 11 Displacements, TTL signals, and currents for a series of coil failure events

Ψ = mode shape matrix
ν = modal state

References

[1] Lyons, J. P., Preston, M. A., Gurumoorthy, R., and Szczesny, P. M., 1994, ''Design and Control of a Fault-Tolerant Active Magnetic Bearing System for Aircraft Engine,'' *Proceedings of the Fourth International Symposium on Magnetic Bearings*, ETH Zurich, 449–454.

[2] Maslen, E. H., and Meeker, D. C., 1995, ''Fault Tolerance of Magnetic Bearings by Generalized Bias Current Linearization,'' IEEE Trans. Magn., **31**, pp. 2304–2314.

[3] Meeker, D. C., 1996, ''Optimal Solutions to the Inverse Problem in Quadratic Magnetic Actuators,'' Ph.D. Dissertation, Mechanical Engineering, University of Virginia.

[4] Maslen, E. H., Sortore, C. K., Gillies, G. T., Williams, R. D., Fedigan, S. J., and Aimone, R. J., 1999, ''Fault Tolerant Magnetic Bearings,'' ASME J. Eng. Gas Turbines Power, **121**, pp. 504–508.

[5] Na, U. J., and Palazzolo, A. B., 2000, ''Optimized Realization of Fault-Tolerant Heteropolar Magnetic Bearings,'' ASME J. Vibr. Acoust., **122**, pp. 209–221.

[6] Na, U. J., and Palazzolo, A. B., 2000, ''Fault-Tolerance of Magnetic Bearings with Material Path Reluctances and Fringing Factors,'' IEEE Trans. Magn., **36**(6), pp. 3939–3946.
[7] Na, U. J., and Palazzolo, A. B., 2001, ''The Fault-Tolerant Control of Magnetic Bearings With Reduced Controller Outputs,'' ASME J. Dyn. Syst., Meas., Control, **123**(2), pp. 219–224.
[8] Matsumura, F., and Yoshimoto, T., 1986, ''System Modeling and Control of a Horizontal-Shaft Magnetic-Bearing System,'' IEEE Trans. Magn., **22**, pp. 197–206.
[9] Bornstein, K. R., 1991, ''Dynamic Load Capabilities of Active Electromagnetic Bearings,'' ASME J. Tribol., **113**, pp. 598–603.
[10] Keith, F. J., Williams, R. D., and Allaire, P. E., 1990, ''Digital Control of Magnetic Bearings Supporting a Multimass Flexible Rotor,'' STLE Tribol. Trans., **33**, pp. 307–314.